Reconstruction of High-energy X-ray Source Using L-shaped Imaging Device

Ruogu She[a,b], Xinge Li[a,*], Na Zheng[a], Haibo Xu[a]

[a] *Institute of Applied Physics and Computational Mathematics, Beijing, China*
[b] *Graduate School of China Academy of Engineering Physics, Beijing, China*

Abstract

The L-shaped imaging devices are used to reconstruct the intensity distribution of the high-energy X-ray source. The physical model considering the penetration effect of X-ray on the imaging device is established, the transmission imaging matrix is constructed, and the algebraic solution method of source intensity reconstruction is presented. The X-ray source with Gaussian distribution is reconstructed. The reconstruction results show that the artifacts and discontinuities in the center of the reconstructed image using L-Edge device can be improved by L-Rolled Edge device, while L-Cylinder device can further improve the reconstruction quality.

Keywords: High-energy X-ray source, Source intensity reconstruction, L-shaped imaging device, Penetration, Transmission imaging matrix

1. Introduction

High-energy X-ray flash radiography can see through the structure, state and evolution process of high-speed moving objects, and is widely used to study the transient evolution process of internal structures of objects under impact loading. It is an indispensable and important diagnostic tool for fast transient processes such as hydrodynamic tests [1, 2, 3, 4, 5]. However, the high-energy X-ray flash imaging system is complex in composition, involving many physical processes, and the imaging quality is also restricted by many factors. The geometrical blur caused by the focal spot size of high-energy

*Corresponding author
Email address: li_xinge@iapcm.ac.cn (Xinge Li)

X-ray source is one of the important reasons for the blur of radiographic images [6]. Therefore, the intensity distribution of high-energy X-ray source and the size of focal spot are important parameters in the process of image analysis. Whether the focal spot parameters of high-energy X-ray source are accurate or not is directly related to whether high-precision reconstructed images can be obtained in theory.

Focal spot measurement is an important part of studying high-energy X-ray flash radiography [7]. The major laboratories engaged in the research of high-energy X-ray flash radiography have carried out the related research on spot size measurement, and representative methods include pinhole method, slit method, edge method, rollbar method and so on [8, 3].

The Atomic Weapons Establishment (AWE) uses cylindrical edge method to measure focal spot on its SuperSwarf flash imaging device [9]. Sandia National Laboratory (SNL) and Lawrence Livermore National Laboratory (LLNL) in the United States use conical pinhole imaging device to measure focal spot on ETA-II accelerator [10]. At the same time, LLNL also carried out measurement based on cylindrical edge method on ETA-II device [11, 12]. Los Alamos National Laboratory (LANL) uses pinhole method to measure focal spot on DARHT-I device [13]. SNL has carried out focal spot measurement on RITS-3 accelerator by using Rolled Edge imaging device [14].

In 2016, Fowler et al. [15] designed the L-Rolled Edge device for imaging based on the "opaque" physical model proposed by Barnea [16], using only one corner of the square hole imaging device, obtained the imaging light and shade information of two dimensions, and gave the two-dimensional intensity distribution of focal spot through image reconstruction. In this paper, based on the "L" configuration device, an imaging physical model considering transmission effect is proposed. Firstly, using L-Edge imaging device, the two-dimensional distribution of the source penetrating the imaging device is obtained, and the intensity distribution of the source is derived by image reconstruction. Through the analysis of the reconstructed images, two improved schemes of the imaging device, L-Rolled Edge and L-Cylinder, are put forward one after another to carry out the source intensity reconstruction.

An outline of the rest of the paper is as follows. In Section 2, we present the mathematical physical modeling and solution. Source intensity reconstruction using L-shaped

imaging device are presented in Section 3. Finally, the conclusion are summarized in Section 4.

2. Mathematical modeling and solution

2.1. Mathematical model of source intensity reconstruction

In the energy range (10keV∼100MeV) of high energy X-ray flash radiography, X-ray has strong penetrability. Therefore, it is necessary to consider the penetrability of high-energy X-ray when measuring the source intensity with the aid of imaging device. The attenuation of X-ray penetrating substance obeys Lambert-Beer law. It is assumed that the X-ray source is an ideal source, that is, an isotropic monomeric point source. The intensity of X-rays emitted from the source, passing through the object and reaching each point on the detector plane can be expressed as

$$I(x,y) = I_0 e^{-\int_0^{d(x,y)} \mu(l)\rho(l)dl}, \tag{1}$$

where I and I_0 are the intensities of X-rays received by the detector with and without objects, $d(x,y)$ is the distance from the point (x,y) on the imaging plane to the source, and $\rho(l)$ and $\mu(l)$ are the density of the material and the mass attenuation coefficient of X-rays in the material at a distance l from the source, respectively.

If the source intensity I_0 obeys a certain distribution $I_0(x',y')$, the intensity of X-ray at any point (x,y) on the imaging plane after penetrating a certain object can be expressed as:

$$I(x,y) = \int\int I_0(x',y') e^{-\int_{(x',y')}^{(x,y)} \mu(l)\rho(l)dl} dx'dy'. \tag{2}$$

Note that the integration area is the whole X-ray source region, and the integration path l is the straight path from the source plane point (x',y') to the imaging plane point (x,y).

If the X-ray source region is discretized as pixels, the integral form of Eq. (2) can be rewritten into the summation form:

$$I(x,y) = \sum_{x'}\sum_{y'} I_0(x',y') e^{-\int_{(x',y')}^{(x,y)} \mu(l)\rho(l)dl}. \tag{3}$$

Further, if the source plane and the imaging plane are respectively discretized in pixels and regarded as one-dimensional vectors, the Eq. (3) can be written in the form of matrix multiplied by vector:

$$\boldsymbol{A}\boldsymbol{x} = \boldsymbol{b}, \tag{4}$$

where the element a_{ij} of matrix $\boldsymbol{A}$ reflects the overall attenuation of the j-th source intensity reaching the i-th pixel on the imaging plane after passing through the imaging device, so it is called the transmission imaging matrix. $\boldsymbol{x}$ is the source intensity to be reconstructed, $\boldsymbol{b}$ is the X-ray intensity measured on the imaging plane.

The above equation is an ideal case when the noise of the imaging system are not considered. If the coefficient matrix $\boldsymbol{A}$ is full rank, the unknown source intensity vector can be obtained by solving linear equations. In practice, noise generally exists, the above equation becomes

$$\boldsymbol{A}\boldsymbol{x} = \boldsymbol{b} + \boldsymbol{n}, \tag{5}$$

where $\boldsymbol{n}$ is the noise of the imaging system.

2.2. Construction of transmission imaging matrix

In the measurement of high energy X-ray source, the imaging layout with geometric magnification ratio $M > 1$ is generally adopted. In this paper, the X-ray source is 15cm away from the center of L-shaped imaging device, and the detector is 120cm away from the center of L-shaped imaging device, that is, the geometric magnification ratio $M = 8$. In view of the current beam control level of accelerator, the radial size of X-ray source can be less than 0.5cm, the source region is set to 1cm $\times$ 1cm. In order to deal with the problem of source drift in practice, the imaging region is expanded from 8cm $\times$ 8cm to 15cm $\times$ 15cm. Considering the computational power, both the source region and the imaging region are discretized to the size of 80×80, then the size of the transmission imaging matrix $\boldsymbol{A}$ is $(80 \times 80) \times (80 \times 80)$, i.e. 6400×6400.

Assuming that the L-shaped imaging device is a homogeneous single medium, the element a_{ij} of the imaging matrix based on the transmission model can be written as

$$a_{ij} = e^{-\mu\rho L((x',y')\to(x,y))} \tag{6}$$

where $L((x', y') \to (x, y))$ is the geometrical length of X-ray passing through the L-shaped imaging device on the path from point (x', y') in the source plane to point (x, y)

in the imaging plane. It can be derived according to the geometric relative position relationship.

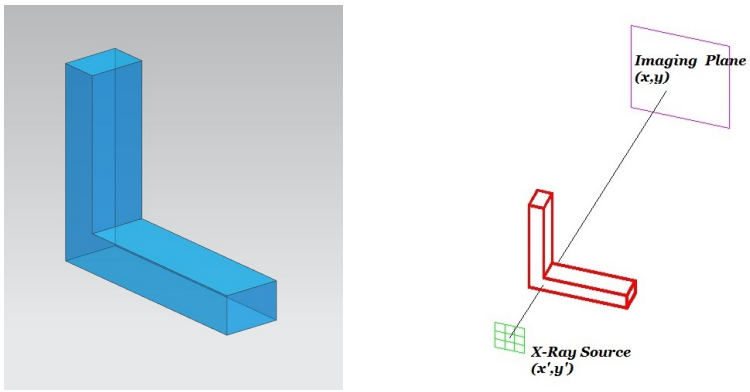

Figure 1: Schematic diagram of X-ray source measurement using L-Edge imaging device.

Taking L-Edge imaging device as an example (see Figure 1), the calculation of $L((x', y') \rightarrow (x, y))$ is as follows. Firstly, the geometric description is defined. Taking the central ridge line of L-Edge (the intersection line of two vertical planes) as the Z-axis, the plane where X-rays are incident on L-Edge (that is, the side near the source) is defined as X_1Y_1 plane, which is divided into I, II, III and IV zones according to the two vertical edges of L-Edge. Similarly, the plane where X-rays are emitted from L-Edge is defined as X_2Y_2 plane (that is, the side near the imaging plane), which is also divided into zones 1, 2, 3 and 4, as shown in Figure 2.

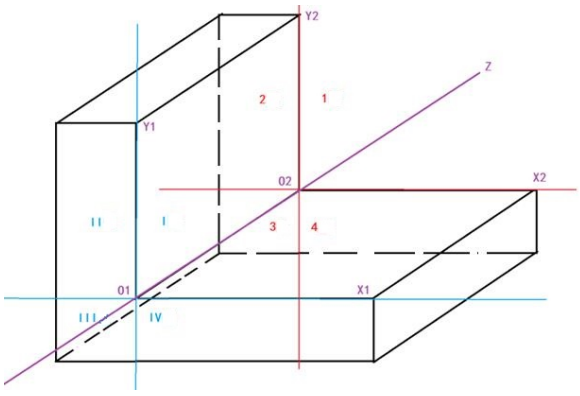

Figure 2: Geometric region partition of L-Edge imaging device.

Table 1: Various cases of calculating geometric length when X-ray passes through L-Edge.

Zone	1	2	3	4
I	$L = 0$	Through $Y_1O_1O_2Y_2$ plane	Through $Y_1O_1O_2Y_2$ plane or $X_1X_2O_2O_1$ plane	Through $X_1X_2O_2O_1$ plane
II	Through $Y_1O_1O_2Y_2$ plane	Calculate the distance between P_1 and P_2 directly	Calculate the distance between P_1 and P_2 directly	Through $Y_1O_1O_2Y_2$ plane and $X_1X_2O_2O_1$ plane
III	Through $Y_1O_1O_2Y_2$ plane or $X_1X_2O_2O_1$ plane	Calculate the distance between P_1 and P_2 directly	Calculate the distance between P_1 and P_2 directly	Calculate the distance between P_1 and P_2 directly
IV	Through $X_1X_2O_2O_1$ plane	Through $Y_1O_1O_2Y_2$ plane and $X_1X_2O_2O_1$ plane	Calculate the distance between P_1 and P_2 directly	Calculate the distance between P_1 and P_2 directly

If X-ray intersects with X_1Y_1 plane P_1 and X_2Y_2 plane P_2, the geometric length of the X-ray in L-Edge can be obtained by discussing the zones where P_1 and P_2 are located in X_1Y_1 plane and X_2Y_2 plane respectively. As shown in Table 1, various cases of X-ray penetrating (or not penetrating) L-Edge are given by enumeration. According to the complexity of treatment, it can be divided into four categories:

1. The simplest is that the X-ray does not intersect with the L-Edge, or the distance in the L-Edge is calculated directly;
2. Secondly, the X-ray passes through one of $Y_1O_1O_2Y_2$ plane and $X_1X_2O_2O_1$ plane. It is necessary to find the intersection point between X-ray and $Y_1O_1O_2Y_2$ plane or $X_1X_2O_2O_1$ plane before calculating;
3. More complicated is that the X-ray passes through $Y_1O_1O_2Y_2$ plane or $X_1X_2O_2O_1$ plane, which needs to be judged.
4. The most complicated is that the X-ray passes through $Y_1O_1O_2Y_2$ plane and $X_1X_2O_2O_1$ plane at the same time. At this time, the path of X-ray in L-Edge is divided into two sections, and the distance in air needs to be subtracted in calculation, as shown in Figure 3.

For the "opaque" model adopted by Barnea et al. [16], it is equivalent to μ being

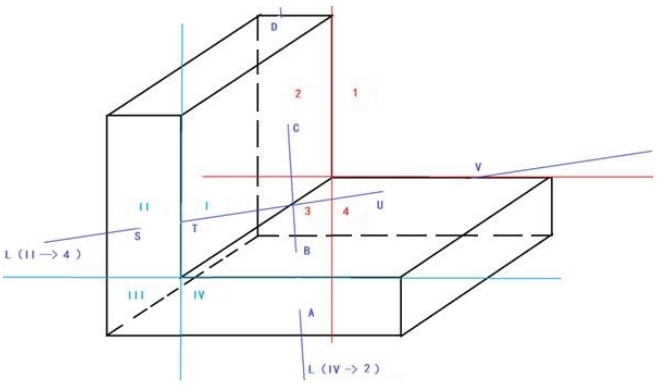

Figure 3: X-ray is divided into two sections in the L-Edge imaging device.

infinity, and the matrix element based on the "opaque" model can be written as:

$$a_{ij} = \begin{cases} 0, & L > 0, \\ 1, & L = 0. \end{cases} \tag{7}$$

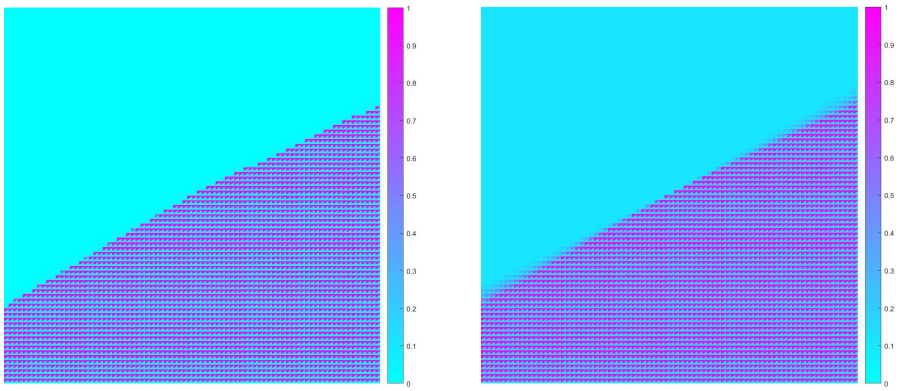

(a) (b)

Figure 4: Imaging matrix of L-Edge imaging device with different physical models. (a) Opaque model; (b) Transmission model considering transmission effect.

Figure 4 shows the imaging matrix of these two models under the same imaging state. It can be seen that the transition between light and shade of opaque model is simple, see Figure 4(a), whereas the imaging matrix in Figure 4(b) changes gradually

after considering the transmission effect, which can more truly reflect the gradual change of X-ray intensity when penetrating L-Edge imaging device.

2.3. Numerical solution method

It is noted that the source intensity reconstruction problem (5) is a typical inverse problem. Considering the ill-posedness of the inverse problem, it is impossible to directly solve the linear equations (5) or its corresponding least squares problem. Only by establishing appropriate constraint criteria can we converge to a reasonable result [17, 18].

The regularization technique is introduced to constrain the possible solution of the ill-posed inverse problem. By constructing a stable functional, the solution of the ill-posed inverse problem is reduced to a functional extremum problem with small regularization parameters. Although the solution may not be unique after the regularization technique is introduced, a relatively well-posed problem is realized to solve the original ill-posed problem. The regularization technique can not only alleviate the ill-posedness of the inverse problem, but also weaken the influence of the noise in the solution and filter the noise, thus improving the reconstruction result. After introducing the regularization technique, solving the algebraic equations (5) is transformed into solving the following optimization problems:

$$\min_{\boldsymbol{x}\geq\mathbf{0}} \|\boldsymbol{A}\boldsymbol{x}-\boldsymbol{b}\|_2^2 + \lambda R(\boldsymbol{x}). \tag{8}$$

Among them, $\|\boldsymbol{A}\boldsymbol{x}-\boldsymbol{b}\|_2^2$ is called fidelity term, which describes the approximation degree of the reconstructed source intensity to the original measurement data; $\lambda R(\boldsymbol{x})$ is the regularization term, that is, the constraint condition imposed artificially. In this paper, the classical Tikhonov regularization model [19] is obtained by assuming that the unknown is the sampled value of a slowly changing function and using the modulus of its first derivative to take the minimum as the criterion:

$$\min_{\boldsymbol{x}\geq\mathbf{0}} \|\boldsymbol{A}\boldsymbol{x}-\boldsymbol{b}\|_2^2 + \lambda\|\nabla\boldsymbol{x}\|_2. \tag{9}$$

This is a nonlinear constrained optimization problem, and we use the practical Constrained Conjugate Gradient (CCG) [20, 21] method to solve it.

3. Reconstruction of source intensity

In this section, we investigate the proposed source reconstruction model considering attenuation by reconstructing Gaussian distributed X-ray source. In the field of nuclear engineering, Monte Carlo (MC) simulation of particle transport is considered to be the closest simulation method to the real experimental state [22, 23]. Therefore, we reconstruct the MC simulation image to test our mathematical and physical modeling and reconstruction method. As shown in Figure 5, set the full-width at half-maximum (FWHM) of X-ray source with Gaussian distribution used in the Monte Carlo simulation as 0.2cm.

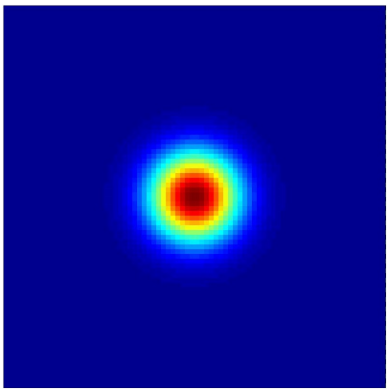

Figure 5: Ground truth of Gaussian distributed X-ray source.

To evaluate of the reconstruction quality, we can have an "eyeball" impression. We can also calculate the relative error between the reconstructed image and the ground truth, that is,

$$Error = \frac{\|\boldsymbol{x} - \boldsymbol{x}_0\|_2^2}{\|\boldsymbol{x}_0\|_2^2}, \tag{10}$$

where $\boldsymbol{x}$ is the reconstructed image, and $\boldsymbol{x}_0$ is the ground truth. In addition, quantitative comparison of the FWHM of the reconstructed image and the ground truth can also help us evaluate the reconstruction effect.

3.1. Source reconstruction using L-Edge

Firstly, we use L-Edge imaging device to take MC simulated photography, in which the L-Edge is made of tungsten with a thickness of 3cm. Figure 6 shows the simulated

image and its reconstructed intensity distribution, and the cross-sectional lines of the reconstructed image in different directions are shown in Figure 7.

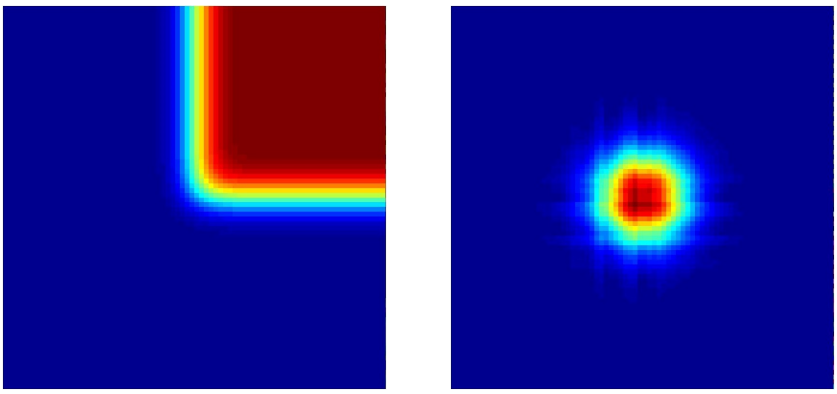

Figure 6: MC simulated image and the corresponding reconstructed Gaussian source.

From the central transverse lines in Figure 7, the size of the reconstructed X-ray source can be obtained, and the FWHM in both horizontal and vertical directions is 0.2cm, which is consistent with the true value. And the relative error between the reconstructed image and the ground truth is 0.0841. However, there are obvious "discontinuities" in the center of the reconstructed source intensity.

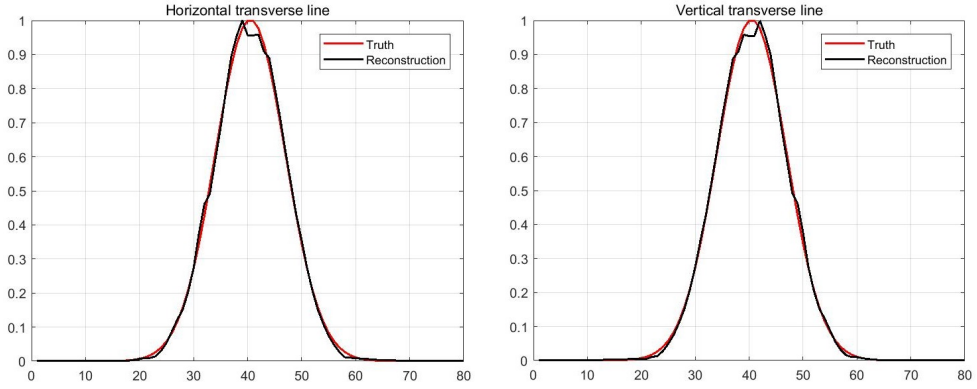

Figure 7: Transverse lines of reconstructed Gaussian source in horizontal and vertical directions.

3.2. Source reconstruction using L-Rolled Edge

In view of the right angle edge of L-Edge imaging device, there is a sudden change of intensity near the edge, which leads to serious artifacts in the reconstructed image. The "discontinuity" characteristic of Edge device has been recognized by relevant researchers in the field of high-energy X-ray source measurement [24]. They point out that in order to improve this "discontinuity", Roll-bar imaging device can be used. Referring to the idea of developing Edge device into Roll-bar device, we improved L-Edge imaging device into L-Rolled Edge imaging device, as shown in Figure 8(a). Specifically, the side surface changes from a plane to a circular arc surface, which avoids the step mutation of source intensity near the side surface.

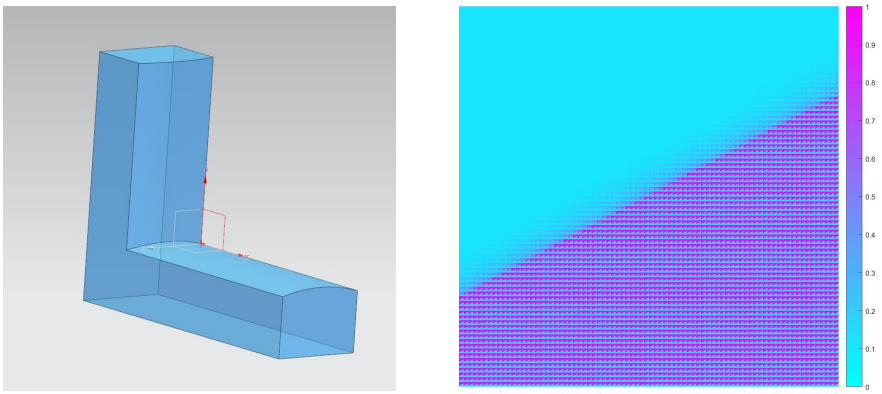

(a) (b)

Figure 8: (a) L-Rolled Edge imaging device; (b) The transmission imaging matrix of the L-Rolled Edge device.

For the selection of radian of L-Rolled Edge device, as shown in Figure 9, the height between the highest point of arc segment and Edge segment is set as h, which is equivalent to the focal spot size of X-ray source. According to the geometric relationship

$$R^2 = L^2 + (R - h)^2,$$

it is easy to get

$$R = \frac{L^2 + h^2}{2h}.$$

In this paper, h is set to 0.2cm, and the arc radius of L-Rolled Edge is 5.725cm.

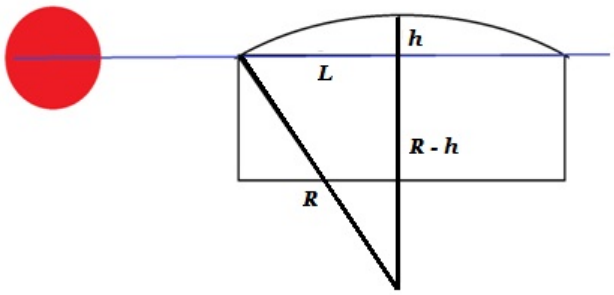

Figure 9: Radian setting of L-Rolled Edge imaging device.

The transmission imaging matrix of the L-Rolled Edge imaging device is shown in Figure 8(b). Compared with Figure 4(b), it is not difficult to find that the transition areas of L-Edge device are mainly distributed on both sides of the central area of the transmission imaging matrix, and there are obvious discontinuities in the central area of the matrix, while L-Rolled Edge device improves the discontinuity of L-Edge, and the whole transition area is distributed in a strip shape, which is more uniform. Moreover, the transition region of the transmission imaging matrix of L-Rolled Edge device is obviously wider and has better continuity, which can provide more information for source intensity reconstruction. Theoretically, it is more conducive to the continuity of reconstructed images.

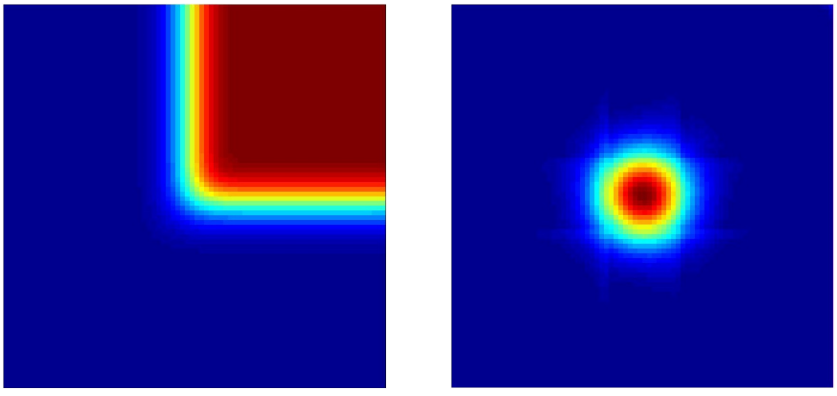

Figure 10: MC simulated image and the corresponding reconstructed Gaussian source.

The MC simulated image using L-Rolled Edge imaging device and its corresponding reconstructed source image are shown in Figure 10. Compared with the right figure in Figure 6, the "L" grid in the center of the reconstructed image using the L-Edge device is significantly improved after using the L-Rolled Edge device, and the latter is closer to the ground truth in the center area. In addition, the relative error of the reconstructed source using L-Rolled Edge device is 0.0765, which is smaller than 0.0841 when L-Edge device is used.

Figure 11 shows the comparison of the reconstructed Gaussian source using L-Rolled Edge device and the ground truth in horizontal and vertical directions, and they are in good agreement. It can be calculated that the FWHM of the reconstructed Gaussian source is 0.2cm, which is consistent with the true value. Moreover, the reconstructed source using L-Rolled Edge device significantly improves the discontinuity on Gaussian peak of the reconstructed source using L-Edge device.

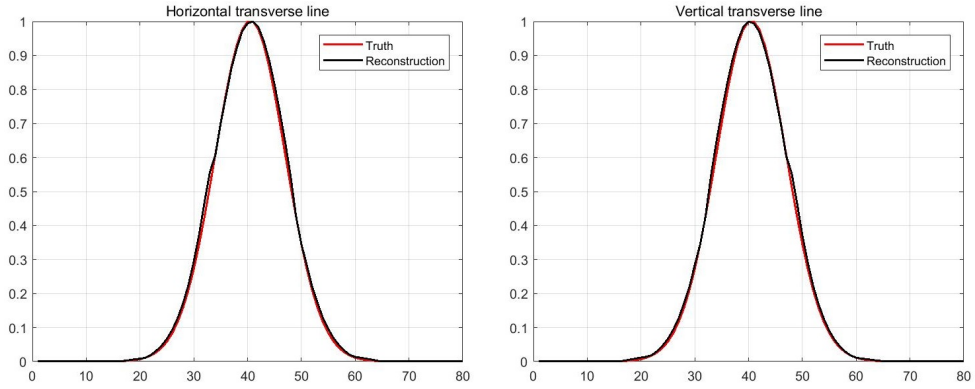

Figure 11: Transverse lines of reconstructed Gaussian source in horizontal and vertical directions.

3.3. Source reconstruction using L-Cylinder

After the L-Edge imaging device is improved to L-Rolled Edge, the imaging quality is greatly improved, especially the "discontinuity" in the central part of the reconstructed Gaussian source is eliminated. However, if we carefully observe the transverse lines of the reconstructed image in horizontal and vertical directions (see Figure 11), we can find that there is still a tiny "discontinuity" at the position deviating from the central peak.

Preliminary analysis shows that the discontinuity may be related to the discontinuity at the junction between the arc section and the Edge section of the L-Rolled Edge device. Therefore, we propose an improved design, that is, the L-Cylinder imaging device is directly formed by splicing two sections of cylinders into an "L" shape, as shown in Figure 12(a).

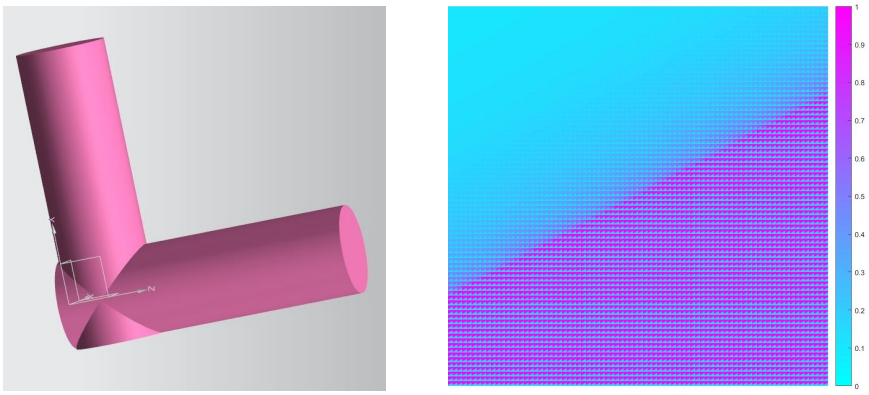

(a) (b)

Figure 12: (a) L-Cylinder imaging device; (b) The transmission imaging matrix of the L-Cylinder device.

The transmission imaging matrix of the constructed L-Cylinder device is shown in Figure 12(b). Compared with Figure 4(b) and Figure 8(b), the transition region of the transmission imaging matrix of the L-Cylinder device is wider and more uniform than that of the L-Edge device and L-Rolled Edge device, which is theoretically more beneficial to the continuity of the reconstructed image.

Figure 13 shows the MC radiographic image with the L-Cylinder device and its corresponding reconstructed intensity distribution, and the cross-sectional lines of the reconstructed image in different directions are shown in Figure 14. It is easy to see that the L-Cylinder imaging device can well reconstruct the intensity distribution of Gaussian source, and accurately measure the FWHM of Gaussian source to be 0.2cm. The L-Cylinder imaging device improves the non-smooth of the reconstructed source with L-Rolled Edge in the lower part of Gaussian peak. Further, the relative error of the reconstructed Gaussian source is 0.0685, which is the smallest among the three imaging

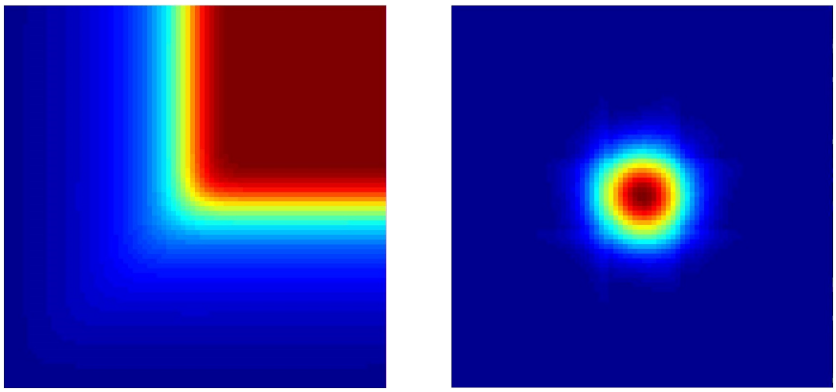

Figure 13: MC simulated image and the corresponding reconstructed Gaussian source.

devices discussed in this paper.

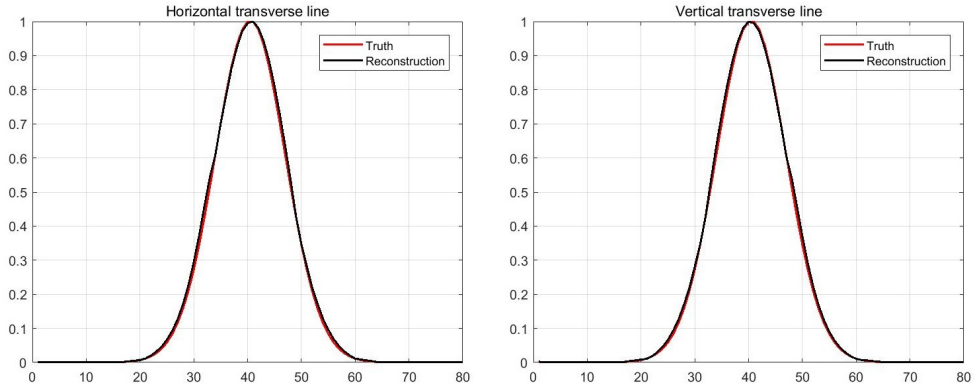

Figure 14: Transverse lines of reconstructed Gaussian source in horizontal and vertical directions.

4. Conclusion

In this paper, a focal spot measurement method of high-energy X-ray source is presented based on source intensity reconstruction using L-shaped imaging device. The physical model considering the penetration effect of X-ray on the imaging device is established, and the transmission imaging matrix is constructed. By introducing regularization technique, the algebraic solution method of source intensity reconstruction is given. The

X-ray source with Gaussian distribution is reconstructed by using the simplest L-Edge imaging device. However, there are serious artifacts in the reconstructed image. In order to improve the quality of source intensity reconstruction, L-Rolled Edge and L-Cylinder imaging devices have been proposed one after another. The reconstruction results show that the artifacts and discontinuities in the center of the reconstructed image can be improved by using the L-Rolled Edge imaging device, while the discontinuities in the reconstructed image can be further improved by using the L-Cylinder imaging device. Then the L-Cylinder imaging device is more suitable for the reconstruction of high-energy X-ray source.

Acknowledgments

This work was supported by the Youth Natural Science Foundation of China (Grant No. 12201057) and the Natural Science Foundation of China (Grant No. 12271053, 11675021).

References

[1] H. Xu, X. Peng, C. Chen, Monte Carlo simulation for bremsstrahlung and photoneutron yields in high-energy X-ray radiography, Chinese Physics B 19 (6) (2010) 062901.

[2] J. Cao, R. Xiao, N. Chen, H. Cao, Z. Yin, Spectral reconstruction of the flash x-ray generated by dragon-i LIA based on transmission measurements, Nuclear Science and Techniques 26 (2015) 040403.

[3] Y. Wang, Z.-Y. Yang, X.-B. Jing, Q. Li, H.-S. Ding, Z.-Y. Dai, Pinhole imaging to observe spatial jitters of a triple-pulse x-ray source on the dragon-ii LIA, Nuclear Science and Techniques 27 (5) (2016) 110.

[4] J. Liu, J. Liu, Y. Jing, B. Xiao, C. Wei, Y. Guan, X. Zhang, Forward model with space-variant of source size for reconstruction on x-ray radiographic image, Nuclear Instruments and Methods in Physics Research Section A: Accelerators, Spectrometers, Detectors and Associated Equipment 883 (2018) 90–95.

[5] Z. Wang, Y. Jing, X. Kang, T. Ding, J. Liu, X-ray radiographs reconstruction based on nonlinear least squares with deconvolution, Nuclear Instruments and Methods in Physics Research Section A, Accelerators, Spectrometers, Detectors and Associated Equipment 929 (2019) 134–141.

[6] S. Portillo, B. V. Oliver, S. Cordova, S. Lutz, Time resolved spot size measurements of the Cygnus rod pinch flash radiographic X-ray source, in: IEEE 34th International Conference on Plasma science, 2007, pp. 238–238.

[7] C. Ekdahl, Characterizing flash-radiography source spots, Journal of the Optical Society of America A Optics Image Science & Vision 28 (12) (2011) 2501–2509.

[8] V. Kaftandjian, Y. M. Zhu, G. Roziere, G. Peix, D. Babot, A comparison of the ball, wire, edge, and bar/space pattern techniques for modulation transfer function measurements of linear x-ray detectors, Journal of X-ray science and technology 6 (2) (1996) 205–221.

[9] T. J. Goldsack, T. F. Bryant, P. F. Beech, S. G. Clough, G. M. Cooper, R. Davitt, R. D. Edwards, N. Kenna, J. McLean, A. G. Pearce, M. J. Phillips, K. P. Pullinger, D. J. Short, M. A. Sinclair, K. J. Thomas, J. R. Threadgold, M. C. Williamson, K. Krushelnic, Multimegavolt multiaxis high-resolution flash X-ray source development for a new hydrodynamics research facility at AWE Aldermaston, IEEE Transactions on Plasma Science 30 (1) (2002) 239–253.

[10] C. E. Crist, S. Sampayan, G. Westenskow, G. Caporaso, T. Houck, J. Weir, D. Trimble, M. Krogh, Time resolved, 2-D hard X-ray imaging of relativistic electron-beam target interactions on ETA-II, in: Proceeding of Linac98, 1998, pp. 195–197.

[11] R. A. Richardson, Optic diagnostic on ETA-II for X-ray spot size, in: Proceedings of the 1999 Particle Accelerator Conference, 1999, pp. 2149–2151.

[12] R. A. Richardson, T. L. Houck, Roll bar X-ray spot size measurement technique, in: Proceeding of the LINAC98, 1998, pp. 161–163.

[13] B. T. McCuistian, D. Moir, E. Rose, H. Bender, C. Carlson, C. Hollabaugh, R. Trainham, Temporal spot size evolution of the DARHT first axis radiographic source, in: Proceedings of EPAC08, 2008, pp. 1206–1208.

[14] A. E. Schach von Wittenau, C. M. Logan, R. D. Rikard, Using a tungsten rollbar to characterize the source spot of a megavoltage bremsstrahlung linac, Medical Physics 29 (8) (2002) 1797–1806.

[15] M. J. Fowler, M. Howard, A. Luttman, S. E. Mitchell, T. J. Webb, A stochastic approach to quantifying the blur with uncertainty estimation for high-energy X-ray imaging systems, Inverse Problems in Science and Engineering 24 (3) (2016) 353–371.

[16] G. Barnea, Penumbral imaging made easy, Review of Scientific Instruments 65 (6) (1994) 1949–1953.

[17] H. W. Engl, M. Hanke, A. Neubauer, Regularization of Inverse Problem, Dordrecht: Springer, 1996.

[18] T. J. Asaki, R. Chartrand, K. R. Vixie, B. Wohlberg, Abel inversion using total-variation regularization, Inverse Problems 21 (6) (2005) 1895–1903.

[19] A. N. Tikhonov, V. Y. Arsenin, Solutions of ill-posed problems, New York: John Wiley & Sons, 1977.

[20] C. R. Vogel, Computational methods for inverse problems, Philadelphia: Society for Industrial and Applied Mathematics, 2002.

[21] H. E. Martz Jr, M. B. Aufderheide III, J. Hall, A. Schach von Wittenau, D. Goodman, C. Logan, J. Jackson, D. Slone, HADES-CCG, A new Tomographic Reconstruction Tool: UCRL-JC-138604, Livermore: Lawrence Livermore National Laboratory, 2000.

[22] S. Agostinelli, J. Allison, K. Amako, et al., GEANT4-a simulation toolkit, Nuclear Instruments and Methods in Physics Research, A 506 (2003) 250–303.

[23] I. Meleshenkovskii, A, T. Ogawa, A. Sari, F. Carrel, K. Boudergui, Optimization of a 9mev elec-

tron accelerator bremsstrahlung flux for photofission-based assay techniques using phits and mcnp6 monte carlo codes, Nuclear Instruments and Methods in Physics Research Section B: Beam Interactions with Materials and Atoms 483 (2020) 5–14.

[24] J. Shi, J. Liu, J. Liu, B. Li, Edge method for measuring source spot-size and its principle, Chinese Physics 16 (1) (2007) 266–271.